Nuclear Instruments and Methods in Physics Research A 397 (1997) 380–390

NUCLEAR INSTRUMENTS & METHODS IN PHYSICS RESEARCH Section A

ELSEVIER

Neutron cross-talk in a multi-detector system

J. Wang[a,*], A. Galonsky[a], J.J. Kruse[a], P.D. Zecher[a], F. Deák[b], Á. Horváth[b], Á. Kiss[b], Z. Seres[c], K. Ieki[d], Y. Iwata[d]

[a]*National Superconducting Cyclotron Laboratory, Michigan State University, East Lansing, MI 48824, USA*
[b]*Department of Atomic Physics, Eötvös University, Puskin utca 5–7, H-1088 Budapest 8, Hungary*
[c]*Research Institute for Particle and Nuclear Physics, Hungarian Academy of Sciences, H-1525 Budapest 114, Hungary*
[d]*Department of Physics, Rikkyo University, 3-34-1 Toshima, Tokyo, 171 Japan*

Received 11 February 1997

Abstract

Two 2 m × 2 m "walls" were built for experiments with two neutrons in the final state. Each wall consists of 25 rectangular cells filled with NE-213 liquid scintillator. The close-packed design of the array makes cross-talk an inevitable contributor to distortion of measurements with this system. For $E_n \leqslant 25$ MeV almost all the detection efficiency comes from n–p scattering, and the simple two-body kinematics can be used as the basis for identifying cross-talk events. A Monte-Carlo code was developed to simulate the detection process. We found that most cross-talk events could be distinguished from real two-neutron events. A test experiment for comparison with the code was performed with neutrons from the ^{7}Li(p, n)^{7}Be reaction at $E_p = 30$ MeV. With this reaction all two-detector coincidences are cross-talk events. Consistency between the experimental data and the simulation results was obtained.

PACS: 29.90.+r,28.20.Cz
Keywords: Neutrons; Cross talk; Neutron detection

1. Introduction

A high-efficiency, position-sensitive, multi-detector system is the ideal apparatus for studying neutrons in the final states of nuclear reactions. Usually such detection systems are arrays of a number of neutron detectors [1–3]. In order to reduce dead space and to be able to measure small-angle coincidences, detectors are put as close to each other as possible. One major concern with these systems is cross-talk between the detectors. Cross-talk happens when a neutron which gives a signal in one detector is scattered into another detector where it again gives a signal. Thus, one neutron appears to be two. Unfortunately, neutron cross-talk inevitably distorts the measurement. The ratio of cross-talk events to real two-neutron events varies with neutron energy and with detector configuration, and it could be very significant on some occasions [2–5]. So, it is very important to understand the effects cross-talk might have before such a detection system is used in experiments, and an effective method is needed to identify cross-talk events.

So far, only a few experiments have been reported on the study of cross-talk [2–5]. Cross-talk probabilities and effects in their specific detection systems were discussed. In this paper, we present a method used to distinguish between cross-talk events and real two-neutron events in the energy region up to ~25 MeV.

A pair of "Neutron Walls", shown in Fig. 1, was built at the National Superconducting Cyclotron Laboratory (NSCL) for experiments in which two neutrons are produced in the final state. Most of the cross-talk events have to be identified and rejected in order for a reliable experimental conclusion to be achieved.

2. The neutron wall facility

In 1991, an experiment was performed [6] to measure the Coulomb excitation of ^{11}Li, an archetypal neutron-halo nucleus. In the experiment, two arrays consisting of 54 cylindrical scintillation detectors, each about 7.6 cm thick and 12.7 cm in diameter, were made to detect the two halo neutrons from ^{11}Li breakup. Although the experiment was somewhat successful, a few drawbacks of the array made us decide to build a better neutron detection system – a pair of neutron walls. These walls

*Corresponding author. Tel.: +1 517 333 6416; fax: +1 517 353 5967; e-mail jwang@nscl.msu.edu.

PII S0168-9002(97)00806-1

are described in Ref. [7]. A brief description follows here. Compared to the array, the walls are larger and use fewer photomultiplier tubes per liter of scintillator. The walls have less dead space and less inactive mass to scatter neutrons. The position resolution is somewhat improved. Each wall consists of 25 rectangular Pyrex cells filled with NE-213 liquid scintillator. Each cell is two meters long, with an internal cross section of 7.62 cm × 6.35 cm. Photomultiplier tubes (PMT) are attached to the ends of a cell. The neutron time-of-flight (TOF) is obtained from the mean time of the PMT signals. The position of a neutron along the cell is determined from the time difference of these signals. Both time and position resolution [7] vary with the light output caused by the neutron's interaction in the scintillator. For a light output equal to that produced by a 1 MeV electron (defined as 1 MeVee), the time resolution (σ_t) is 0.8 ns. It reduces to 0.4 ns for a light output over 4 MeVee. The position resolutions (σ_p) for these light outputs are 6 and 3 cm, respectively. The neutron detection efficiency for one wall is 11% for 25 MeV neutrons at a threshold of 1 MeVee. In experiments with the neutron walls, many of the neutrons produce the same amount of light as γ-rays. Therefore, the walls are capable of pulse-shape-discrimination to distinguish between neutron events from γ-ray events.

In most experiments, the two walls are used with one wall behind the other as shown in Fig. 1. There are two advantages of using this configuration: (1) It enhances the detection efficiency. (2) It has the capacity of detecting neutrons emitted with small relative angles. In order to explain the second advantage, consider the extreme case – two identical neutrons emitted from a source with zero relative angle. If only one wall is used, the two neutrons will be detected in the same cell at the same time with a certain probability. Unfortunately, we cannot distinguish them because what we detect is just the superposition of two pulses. However, if the two walls are used, it is possible, that one neutron makes a pulse in one wall and the other neutron makes a pulse in the other wall. Since they are detected in different cells, it is not hard to distinguish them and to determine their relative angle, even if it is 0°.

The choice of the distance between the target and the wall depends on the neutron energy, which is measured by TOF, counting rate and the requirement of angular coverage. If the front wall, the one close to the target, is 5 m from the target, the energy resolution is about 3% for 25 MeV neutrons, and the wall subtends an angle of about 23°. A large distance between the front wall and the back wall is advantageous for good cross-talk identification.

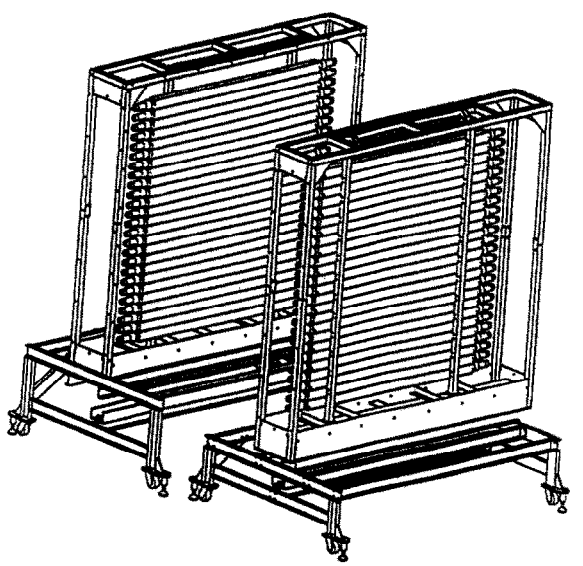

Fig. 1. Picture of the neutron walls without their aluminum protective covers. Each wall consists of 25 rectangular cells filled with NE-213 scintillator. Each cell, with photomultipliers at the ends, has a dimension of $7.62 \times 6.35 \times 200\,cm^3$. The walls are movable so that they can be set at the desired positions.

3. Cross-talk in the neutron walls

3.1. Cross-talk types

In this paper, cross-talk events are classified into two categories as illustrated in Fig. 2.

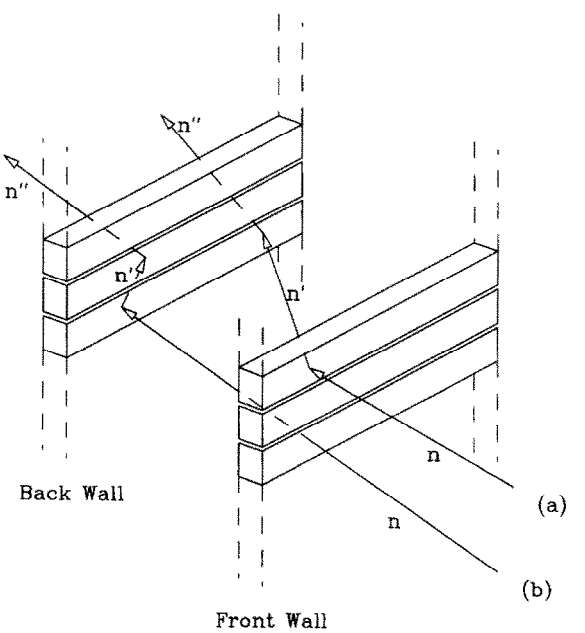

Fig. 2. The two types of cross-talk in the neutron walls. Type (a) cross-talk makes one signal in the front wall and another in the backwall. Type (b) cross-talk makes both signals in either one of the two walls.

(a) Cross-talk between the two walls, where a neutron makes one signal in the front wall and one signal in the back wall.

(b) Cross-talk within one wall, where a neutron makes two signals in different cells of the same wall. We anticipate that most of the cross-talk events within one wall happen in neighboring cells, because a neutron has to scatter a large angle in order to reach distant cells, and the cross section for neutron scattering decreases significantly with increasing angle.

3.2. Cross-talk effects

Cross-talk affects a two-neutron experiment in two ways.

(a) It causes overestimation of neutron coincidences. Because cross-talk events are really one-neutron events, the number of neutron coincidences is enhanced by cross-talk events if these events are not identified as cross-talk events.

(b) The cross-talk within one wall distorts the small angle correlation (Refer to the n–n relative momentum distribution in Ref. [6]). Since a neutron cross-talk event within one wall most probably happens in neighboring cells, the event looks like two neutrons emitted from the source with a small relative angle. If cross-talk events are not identified, the small-angle correlation is falsely enhanced.

Obviously, we have to reject as many cross-talk events as possible to avoid these negative effects.

4. Cross-talk identification

4.1. Neutron detection in liquid scintillator

It is useful to look at the main interactions between neutrons and scintillator materials before we introduce cross-talk identification.

Since the composition of the scintillator is hydrogen and carbon, neutrons usually interact with scintillator through the six processes listed in Table 1. Because #4 and #6 have no neutrons in the final states, they make no contribution to cross-talk.

Neutrons are detected with the scintillation light caused by energy loss of charged particles – protons, carbon nuclei and α particle – which are produced in #s 1, 2, 3 and 5. In Fig. 3, the light response curves for these charged particles are plotted, based on the data from Verbinski et al. [8]. Although #2, n-^{12}C elastic scattering, has the largest cross section, it hardly contributes to neutron detection because of the very low light response for carbon nuclei. Similarly, #3 gives little contribution to cross-talk effects when the γ-rays escape the scintillator undetected. Even if a γ-ray produced in #3 is detected, it can be ruled out by n–γ discrimination.

Table 1
The interactions between neutrons and the nuclei in liquid scintillators – protons and carbon. σ_R is the reaction cross section. The data are from the code by Cecil et al. [9]

	Interactions	σ_R(24 MeV)
1	n + p → n + p	0.406*b*
2	n + C → n + C	0.900*b*
3	n + C → n′ + C + γ(4.44 MeV)	0.104*b*
4	n + C → He + Be − 5.71 MeV	0.048*b*
5	n + C → n + 3α − 7.26 MeV	0.210*b*
6	n + C → p + B − 12.59 MeV	0.100*b*

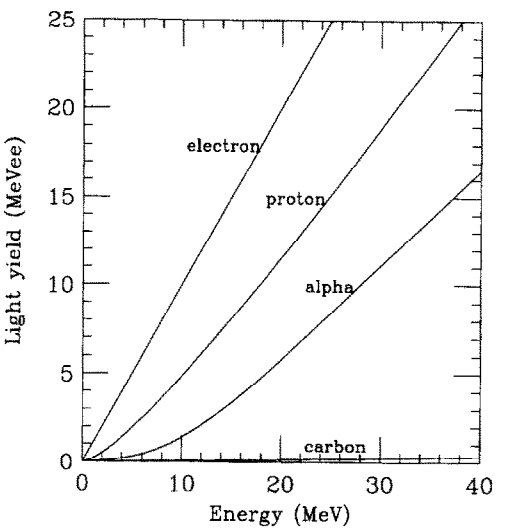

Fig. 3. The light response for electrons, protons, alphas and carbon nuclei in liquid scintillator. 1 MeVee is equal to the light produced by a 1 MeV electron. The data are from Verbinski et al. [8].

Process #5, which has a reaction threshold of 7.86 MeV, produces low-energy α-particles. Because of the low output of these particles, #5 does not play an important role in neutron detection below 25 MeV.

In conclusion, among those processes with neutrons in the final states, n–p scattering is dominant for neutron detection if $E_n \leqslant 25$ MeV. Therefore, n–p scattering is also the primary source of cross-talk.

4.2. 2-body kinematics

Since n–p elastic scattering is the major contributor to cross-talk, the well-known 2-body kinematics, illustrated in Fig. 4, becomes our basis for neutron cross-talk identification. In this figure, n is the incident neutron, n′ is the scattered neutron, p is the recoil proton, and θ represents the neutron's scattering angle. If we assume $m_n = m_p$,

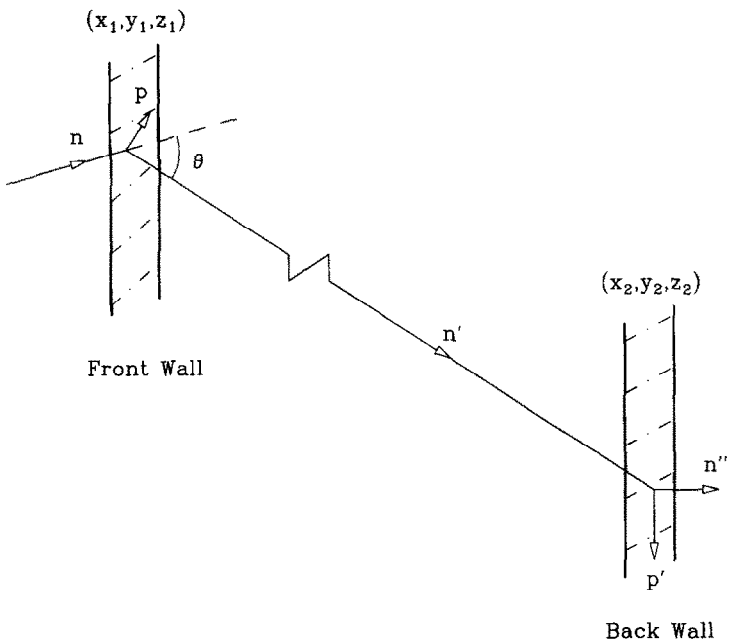

Fig. 4. An example of cross-talk between the front wall and the back wall. The neutron makes one signal in a cell of the front wall and another one in a cell of the back wall. The position of each scattering is expressed by (x,y,z). The scattering in the front wall follows the 2-body kinematics given by Eqs. (1) and (2) in the text.

energy and momemtum conservation result in the following equations:

$$E'_n = E_n - E_p, \tag{1}$$

$$E'_n = E_n \times \cos^2\theta. \tag{2}$$

The above equations exhibit the correlation between neutron energy, proton energy and the scattering angle. If E_n and E_p are known, E'_n and $\cos\theta$ can be determined.

In the next three sections, we show how the 2-body kinematics engenders three signatures of cross-talk.

4.3. $(\cos\theta)_c - (\cos\theta)_m = 0$ (*signature # 1 of cross-talk*)

Fig. 4 shows a typical cross-talk event between the front wall and the back wall. There are two scatterings detected in this case. For the first scattering, we measure by TOF the incoming neutron's energy – E_n, the light output of the recoil proton – L_p, and the position of the scattering – (x_1, y_1, z_1). These coordinates are defined in such a way that the x and y-axis, vertical and horizontal, respectively, to the cells, are in the plane of a wall, and the z-axis points from the neutron source to the walls. The neutron source also serves as the origin of the coordinates. If a neutron is detected in a certain cell, x_1 is given by the position of the cell's center, y_1 is given by the time difference of the signals at the ends of the cell, and z_1 is the distance between the source and the front wall. The recoil proton's energy E_p can be extracted from the light output in the NE-213 scintillator by using its light response function. The response function for charged particles was determined by fitting the light yield data of Verbinski et al. [8] with an empirical expression of the form:

$$L = a \cdot (1 - \exp(-b \cdot E^c)) + d \cdot E + f. \tag{3}$$

The light output L is in the unit MeVee (the light produced by an electron of 1 MeV), and E is in MeV. E denotes the energy of charged particles. The parameters – a, b, c, d, f – which give the best fit for protons, alpha particles and carbon nuclei, are listed in Table 2. After E_n and E_p are determined, we can calculate the scattered neutron's energy by energy conservation, $E'_n = E_n - E_p$. Then Eq. (2) is used to obtain the value of $\cos\theta$. We call it the "calculated" $\cos\theta$, $(\cos\theta)_c$.

$$(\cos\theta)_c = (E'_n/E_n)^{1/2}. \tag{4}$$

For the second scattering, we determine its position – (x_2, y_2, z_2). From the position in the front wall, $\boldsymbol{u}_1 = (x_1, y_1, z_1)$ and the position in the back wall, $\boldsymbol{u}_2 = (x_2, y_2, z_2)$, we can obtain the "real" value of $\cos\theta$. We call it the "measured" $\cos\theta$, $(\cos\theta)_m$.

$$\boldsymbol{u}_{21} = \boldsymbol{u}_2 - \boldsymbol{u}_1 \rightarrow (\cos\theta)_m = \boldsymbol{u}_1 \cdot \boldsymbol{u}_{21}/|\boldsymbol{u}_1||\boldsymbol{u}_{21}|, \tag{5}$$

Table 2
The best parameters of the light response function $L = a \times (1 - \exp(-b \times E^c)) + d \times E + f$ for protons, alpha particles and carbon nuclei

Particles	a	b	c	d	f
p	−5.6375	0.115	0.838	0.7875	0.015
α(< 5 MeV)	−6.1643	−0.001	2.2	0.01585	0.0
α(> 5 MeV)	−5.2688	0.0872	1.22	0.543	0.0
C	0.0	0.0	0.0	0.017	0.0

If the event is a cross-talk event, $(\cos\theta)_c$ should equal $(\cos\theta)_m$, i.e., $(\cos\theta)_c - (\cos\theta)_m$ should be zero. Due to the uncertainty in measuring all the quantities. e.g., energies and positions, the $(\cos\theta)_c - (\cos\theta)_m$ distribution function is not a δ-function at $(\cos\theta)_c - (\cos\theta)_m = 0$, but a peak with a width. The spread of the peak is related to the energy resolution and the position resolution of the detection system.

Unless cross-talk events are identified, we cannot tell cross-talk events from real 2-n events in which two neutrons from the source are detected. Shown in Fig. 5 is a real 2-n event between the front wall and the back wall. If we assume that this is a cross-talk event, we expect θ, which is calculated on the basis of 2-body kinematics, to be the neutron's scattering angle. However, the positions of the two interactions give θ'. The two angles are different because they are not correlated by 2-body kinematics. Since the cosine of θ gives $(\cos\theta)_c$ and the cosine of θ' gives $(\cos\theta)_m$, $(\cos\theta)_c - (\cos\theta)_m$ is not equal to 0. So, for real 2-n events, $(\cos\theta)_c - (\cos\theta)_m$ would not form a peak at zero. Instead, $(\cos\theta)_c - (\cos\theta)_m$ should be distributed over the range allowed by the geometry of the neutron walls.

4.4. $\Delta T_c - \Delta T_m = 0$ (*signature #2 of cross-talk*)

In part (3), we established the first signature of cross-talk in terms of $(\cos\theta)_c - (\cos\theta)_m$. Similarly, in this part, we will establish the second signature of cross-talk from another aspect of the 2-body kinematics of n–p scattering. Referring to the example of cross-talk in Fig. 4, we calculate the scattered neutron's energy E'_n from the incident neutron energy E_n and the recoil proton energy E_p with Eq. (1). From E'_n, we calculate the velocity of the scattered neutron v'_n. L_{12} is the flight path of the scattered neutron between $\boldsymbol{u}_1 = (x_1, y_1, z_1)$ in the front wall and $\boldsymbol{u}_2 = (x_2, y_2, z_2)$ in the back wall. If it is a cross-talk event, determination of v'_n and L_{12} gives the flight time of the scattered neutron. We call it the "calculated" ΔT, ΔT_c. The following is the logic flow leading to ΔT_c:

$$\left.\begin{array}{l} E_n,\ E_p \rightarrow E'_n \rightarrow v'_n \\ \boldsymbol{u}_1,\ \boldsymbol{u}_2 \rightarrow L_{12} = |\boldsymbol{u}_1 - \boldsymbol{u}_2| \end{array}\right\} \Rightarrow \Delta T_c = L_{12}/v'_n \qquad (6)$$

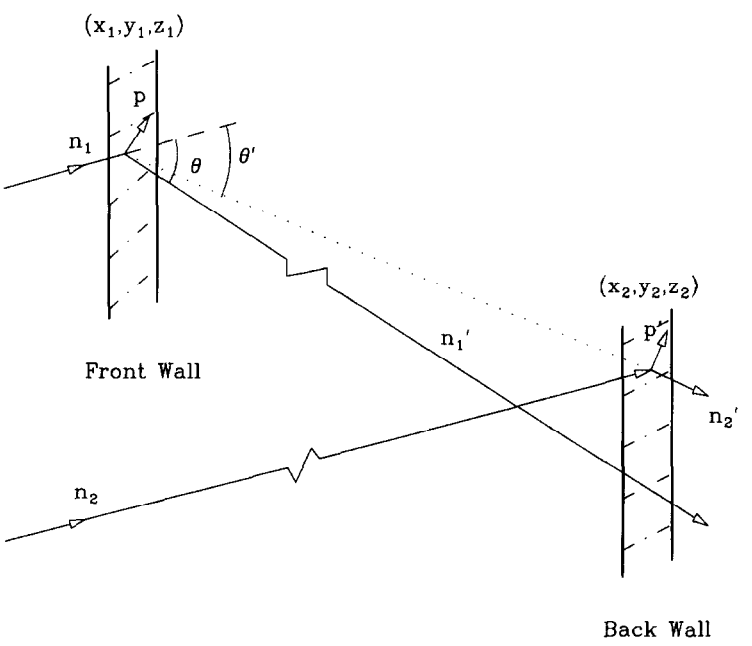

Fig. 5. An example of real 2-n event between the front wall and back wall. If we assume this is a cross-talk event, θ should be the neutron's scattering angle according to 2-body kinematics. However, the positions of the two scatterings give θ'. Unlike cross-talk events, the two angles are not correlated for real 2-n events.

On the other hand, the actual time difference can be measured by taking the difference between the TOF of the first scattering $(TOF)_1$, and that of the second scattering $(TOF)_2$. We call it the "measured" ΔT, ΔT_m.

$$\Delta T_m = (TOF)_2 - (TOF)_1 \quad (7)$$

For neutron cross-talk events, ΔT_c should be equal to ΔT_m. The $\Delta T_c - \Delta T_m$ distribution function peaks at zero, but again, due to uncertainties of measurements, the peak has a finite width. Since the two scatterings in a real 2-*n* event are not correlated by 2-body kinematics, ΔT_c does not represent the time difference between them. Hence $\Delta T_c - \Delta T_m$ tends to be random for real 2-*n* coincidences.

4.5. $E'_p \leqslant E'_n$ (*signature # 3 of cross-talk*)

In a cross-talk event, the energy E'_p of the recoil proton in the back wall should be less than or equal to the energy E'_n of the neutron coming from the first scattering in the front wall. In a real 2-*n* event, that is not necessarily true because the two scatterings involve two different neutrons from the source. E'_p could be larger than E'_n. So, $E'_p \leqslant E'_n$ becomes the third signature of cross-talk.

We have introduced the three signatures of cross-talk between the front wall and the back wall. Cross-talk within one wall has all three signatures, too. But the first signature, $(\cos\theta)_c - (\cos\theta)_m = 0$, is not used because the geometric configuration of the cells in one wall destroys our ability to determine $(\cos\theta)_m$, as illustrated in Fig. 6.

4.6. *Monte-Carlo simulation*

In order to check the signatures of cross-talk, a Monte-Carlo code has been written based on the code developed by Cecil et al. [9]. Our modifications of the code are listed below:

(a) Implementation of measured neutron differential cross sections for n–p and n–C elastic scattering. The data were retrieved from the National Nuclear Data Center (NNDC). The energy dependence of the angular distributions was parameterized. Parameter interpolation is used in the code to get the differential cross section for continuous energy values.

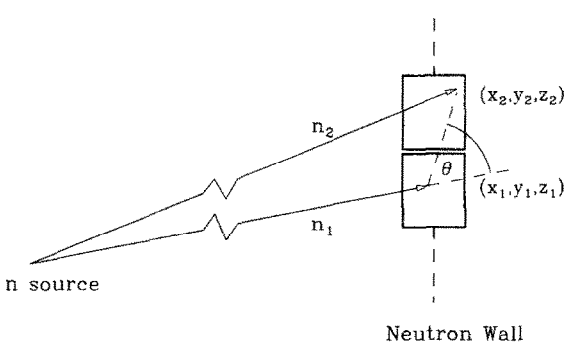

Fig. 6. Side view of two neutrons detected in neighboring cells. Because it is impossible to determine the exact positions where the neutrons scattered, θ can vary from almost 0° to 180°.

(b) Consideration of a neutron's reaction in the Pyrex glass cell. The Pyrex is composed of oxygen, silicon, boron, sodium and aluminium, and more than 80% of the material is oxygen and silicon. In order to simplify the simulation, B and Al are treated as O and Si, respectively. Since the atomic mass number of Na is between those of O and Si, half Na is treated as O and half is treated as Si. All data, including total cross sections with O and Si and differential cross sections for elastic scattering with O and Si, are obtained from the NNDC.

(c) Input of the geometric configuration of the detection system. In the original code only one detector was treated. The modified code deals with 50 detectors.

(d) Fitting of light response function. Parameters for different charged particles are in Table 2.

A study of neutron cross-talk was conducted with the code to simulate its effect on a measurement of the two neutrons from ^{11}Li breakup. ^{11}Li has two loosely bound halo neutrons. When ^{11}Li goes through a strong Coloumb field [6], it may absorb a virtual photon with an energy greater than the two-neutron separation energy of ^{11}Li, and hence break up into two neutrons and a ^{9}Li, The difference between the energy of the photon and the two-neutron separation energy is referred to as the decay energy. The two neutrons and ^{9}Li are assumed to share the decay energy according to the momentum distribution in 3-body phase space.

In the code, the two neutrons are traced as they go through the neutron walls. If both neutrons are detected, we have a real 2-neutron event. If only one of the neutrons is detected, but in two different cells, we have a cross-talk event. This simulation makes it possible for us to make a direct comparison between real coincidence events and cross-talk events. Furthermore, it can show the reliability of our methods to identify cross-talk events from real 2-n events. The ^{11}Li beam energy we used in the code is 25 MeV/u. We chose 1.0 MeV as the ^{11}Li decay energy. The neutron walls are set at 0 relative to the beamline and perpendicular to it. The first wall is 5 m from the source. The second wall is 1 m behind the first one. The results of the simulation are shown in Table 3 and Fig. 7. Table 3 gives the number of real 2–n events and cross-talk events detected by the neutron walls when one million ^{11}Li breakups occur. The events are categorized into the events between the two walls, the events within the front wall and the events within the back wall. In Fig. 7, Plot (a) gives $(\cos\theta)_c - (\cos\theta)_m$ distributions for the 2-neutron coincidence events between the two walls. The solid histogram is for all the 2-n events, both real and apparent, whereas the dashed histogram is for the real 2-n coincidences only. Their difference is the distribution

Table 3
Number of 2-n events detected by the neutron walls when one million ^{11}Li breakups were simulated

Between the two walls	
Total 2-n events	27390
Real events	20985
Cross-talk events	6405
Within the front wall	
Total 2-n events	16194
Real events	13132
Cross-talk events	3062
Within the back wall	
Total 2-n events	10865
Real events	8335
Cross-talk events	2530

for cross-talk events. The cross-talk events form a peak at zero, as we expected. Plot (b) gives $\Delta T_c - \Delta T_m$ distributions for the 2-n events between the two walls and plot (c) gives $\Delta T_c - \Delta T_m$ distributions for the 2-n events within one wall. As in plot (a), distributions for all the 2-n coincidence events and for the real 2-n coincidence events are plotted. Again, the peaks around zero are the result of cross-talk.

The spread of the peaks for the cross-talk events is due to the uncertainty of the measurements. The uncertainty parameters used in the code are: time resolution (σ_t) = 0.4 ns, position resolution (σ_p) = 5 cm, light collection uncertainty (σ_l) = 10% for a light output of 1.0 MeVee and the attenuation length in the NE-213 = 160 cm. Among the parameters, light collection uncertainty is due to the statistical fluctuation in the amount of light collected by the phototubes. It is proportional to $1/L^{1/2}$, where L, the light produced by charged particles, such as protons, alpha particles and carbon nuclei, is in units of MeVee. The asymmetry of the peaks in the $\Delta T_c - \Delta T_m$ distributions for cross-talk events is due to neutron multiple scattering. Sometimes neutron scattering with C or H, especially with C, generates too little light to be detected. However the deflected neutron may generate enough light to be detected in the next scattering in the scintillator. Although multiple scattering can make $(\cos\theta)_m$ either larger or smaller, multiplier scattering always increases the neutron flight path, and hence can only increase ΔT_m. That is why the $(\cos\theta)_c - (\cos\theta)_m$ peak is symmetrical while the $\Delta T_c - \Delta T_m$ is asymmetric, with a tail on the negative side.

The results of the simulation clearly show us the differences between cross-talk events and real 2-n events. Based on these differences, as well as $E'_p \leqslant E'_n$, cross-talk identification can be achieved.

4.7. *Steps for neutron cross-talk identification*

From the signatures described in Sections 4.3–4.5, we found that cross-talk events form a peak at zero in both the $(\cos\theta)_c - (\cos\theta)_m$ distribution and the $\Delta T_c - \Delta T_m$ distribution, and they have the property that $E'_p \leqslant E'_n$. Therefore, we can reject cross-talk events by setting gates around zero on the two distributions and by requiring $E'_p \leqslant E'_n$. The setting of the gate should be determined by the spread of the distribution of the cross-talk events. For convenience of explanation, we denote G_1 as the gate on

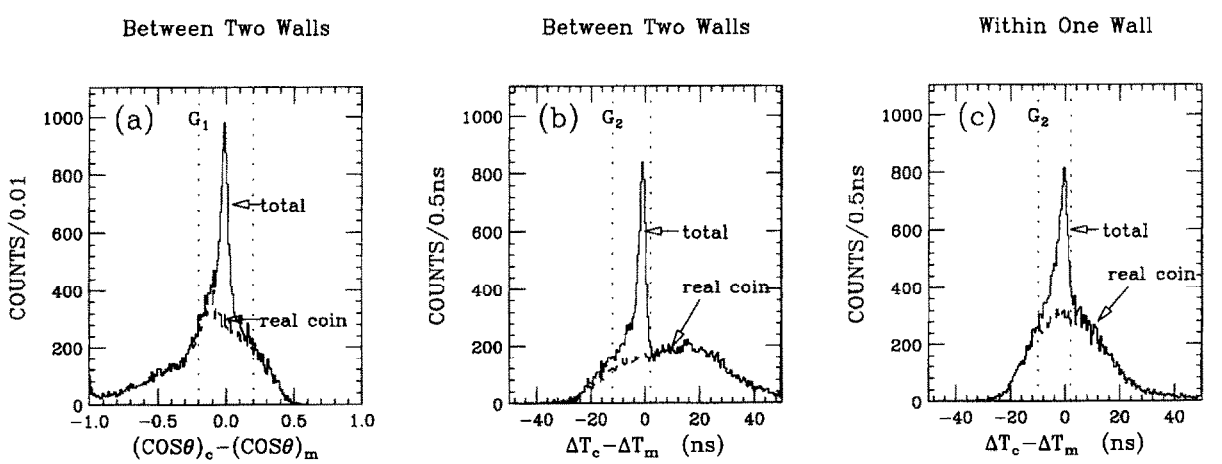

Fig. 7. The results of a Monte-Carlo simulation in which two neutrons from ^{11}Li breakup are detected by the neutron walls. Given by the solid histograms, "total" represents all the two-neutron events detected by the walls. Given by the dashed histograms. "real coin" represents the real two-neutron coincidences. G_1, G_2 are the gates used to reject the cross-talk events. (a) $(\cos\theta)_c - (\cos\theta)_m$ distribution for the events between the two walls. (b) $\Delta T_c - \Delta T_m$ distribution for the events before the two walls. (c) $\Delta T_c - \Delta T_m$ distribution for the events within either the front wall or the back wall.

$(\cos\theta)_c - (\cos\theta)_m$ and G_2 as that on $\Delta T_c - \Delta T_m$, as indicated in Fig. 7. C_3 is the third condition that $E'_p \leqslant E'_n$. From the result of the ^{11}Li breakup simulation, we can see that there are some real 2-n events mixed with cross-talk events in the cross-talk region. When we reject cross-talk events, we cannot avoid losing some real 2-n coincidence events. In choosing gates, the goal, of course, is to reject most of the cross-talk events and keep most of the real 2-n events. It is important to realize that a 2-n event is considered a cross-talk event only if it is found in both of the gates G_1, G_2 and it satisfies C_3. For real 2-n events the three conditions are not correlated. Even so, some real 2-n events may satisfy all three conditions. For events within the front wall or within the back wall, only G_2 and C_3 are used (refer to Section 4.5).

Here are the three steps to tell if an event between the walls is a cross-talk event after G_1, G_2 are chosen and C_3 is considered.

(a) Calculate $(\cos\theta)_c - (\cos\theta)_m$. Is it within G_1?

(b) Calculate $\Delta T_c - \Delta T_m$. Is it within G_2?

(c) Calculate E'_n and E'_p. Does it satisfy C_3?

Only if the answer is "yes" for all the three steps, is the event identified as a cross-talk event. For 2-n events with one wall, only the last two steps are used.

In the simulation for ^{11}Li breakup, the method was used to identify the cross-talk events. G_1 was set from -0.2 to 0.2 (Fig. 7). G_2 was set from -12 to 2 ns. The results of the simulation for 2-n events between the two walls are listed in Table 4. In this particular simulation, we had 27 390 2-n events, of which 20 985 were real 2-n events and 6405 were cross-talk events. There were 7340 events satisfying G_1, G_2 and C_3, of which 5013 were cross-talk events and 2327 real events. By taking the 7340 events out as cross-talk events, we rejected 78.3% of the cross-talk events and at the same time lost only 11.1% of the real 2-n events. This reduced the cross-talk impurity from 23.4 to 6.9%. Using G_2 and C_3, we also identified the cross-talk events within one wall. G_2 was set from -10 to 2 ns. Following the same procedure used for 2-n events between the two walls, we rejected 79.6% of the cross-talk events and lost 26.8% of the real 2-n events. The cross-talk impurity was reduced from 22.9% to 7.7%. Because only two conditions can be used for 2-n events within one wall, we lose more real events in this case than we do in the case for 2-n events between the two walls.

Since cross-talk identification depends on the three gates, the success of the method depends on how the gates are set. The gates depend on the spread of the $(\cos\theta)_c - (\cos\theta)_m$ and $\Delta T_c - \Delta T_m$ distributions for cross-talk events. The spread is going to be different for different detection systems. For any system, there will always be the need for a software trade-off between size and purity of the event set. The higher the purity demanded, the greater the number of good events sacrificed. The choice is made by the experimenter.

Table 4
Results of the simulation of ^{11}Li breakup for 2-n events between the two walls. G1 and G2 are the gates set on $(\cos\theta)_c - (\cos\theta)_m$ and $\Delta T_c - \Delta T_m$ distributions, respectively, shown in Fig. 7. C3 is the coordination that $E'_p \leqslant E'^n$, explained in Section 4.5. In experiments, all the 2-n events which fall in G1, G2 and satisfy C3 are rejected as cross-talk events

Real events	20985
Cross-talk events	6405
Total no. of events	27390
Real events	
in G1	10995
in G2	3981
satisfy C3	10931
in G1 and in G2	2746
in G1 and in G2 and satisfy C3	2327
retained real events	18658
Cross-talk events	
in G1	5904
inG2	5474
satisfy C3	6251
in G1 and in G2	5118
in G1 and in G2 and satisfy C3	5013
retained cross-talk events	1392
% of identified cross-talk	78.3%
Loss of real events	11.1%
Cross-talk percentage of total 2-n events (before)	23.4%
Cross-talk percentage of total 2-n events (after)	6.9%

5. Experiment

5.1. Setup

A test experiment was performed at the NSCL using the reaction:

$$^7\mathrm{Li} + \mathrm{p} \rightarrow \mathrm{n} + {}^7\mathrm{Be} - 1.64\ \mathrm{MeV} \quad (8)$$

In this reaction, only one high-energy neutron is produced. Therefore, all the 2-n events detected by the neutron walls were cross-talk events. The purpose of the experiment was to check if our simulation code gives the right prediction, i.e. to see if the $(\cos\theta)_c - (\cos\theta)_m$ and $\Delta T_c - \Delta T_m$ distributions for cross-talk events obtained from the experiment agree with those simulated by our computer codes. The experimental set up shown in Fig. 8. The neutron walls were set at 35° relative to the beam-line. Concrete blocks were placed between the down-stream beam pipes and the neutron walls to shield the walls from neutrons produced by target-scattered protons striking the pipes. Neutrons were produced by bombarding a 0.5 mm ^{7}Li target with 29.8 MeV protons

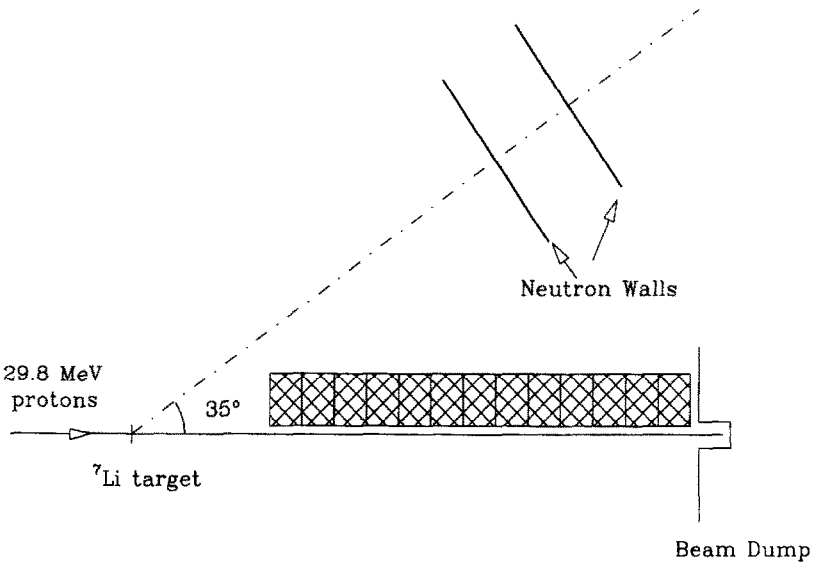

Fig. 8. Layout of the ^{7}Li(p, n) experiment. The front wall was placed 5 m from the target, 35° relative to the beamline. The second wall was 1 m behind the first one. The shaded area was a stock of concrete blocks.

extracted from K1200 cyclotron. Forty of the 50 glass cells were used in the experiment, but only 20 cells were analyzed due to problems with the pulse-shape-discrimination circuitry for the other 20 cells. Of the 20 working cells, there were 8 cells in the front wall, from no. 5 to no. 12, counting from the bottom. The other 12 cells were in the back wall from no. 9 to no. 20.

5.2. Data analysis

Fig. 9 shows the neutron TOF spectrum for cell no. 7 in the front wall. The mean time of the two signals at the ends of the cell gives the start. The downscaled cyclotron radio frequency time gives the stop. Neutrons under the sharp peaks are from the ^{7}Li(p, n) reaction which goes to either the ground state or the first excited state of ^{7}Be. The two states have an energy difference of only 0.43 MeV. The resolution of the system is not able to distinguish between the two states. The energy of the neutrons under the peaks can be determined from their reaction angles by 2-body kinematics. The energy loss of the protons in the target was 0.4 MeV. Using an average of 0.2 MeV, the energy of the neutrons under the sharp peaks detected in the front neutron wall ranges from 25.4 to 27.3 MeV, depending on where the neutrons strike the wall, i.e., on the reaction angle. The neutrons outside the sharp peaks in Fig.9 are predominantly from the reaction

$$^7\mathrm{Li} + \mathrm{p} \rightarrow \mathrm{n} + {}^3\mathrm{He} + {}^4\mathrm{He} - 3.23\ \mathrm{MeV} \qquad (9)$$

The 3-body final state makes the E_n spectrum a continuum. The energies of these neutrons were measured by

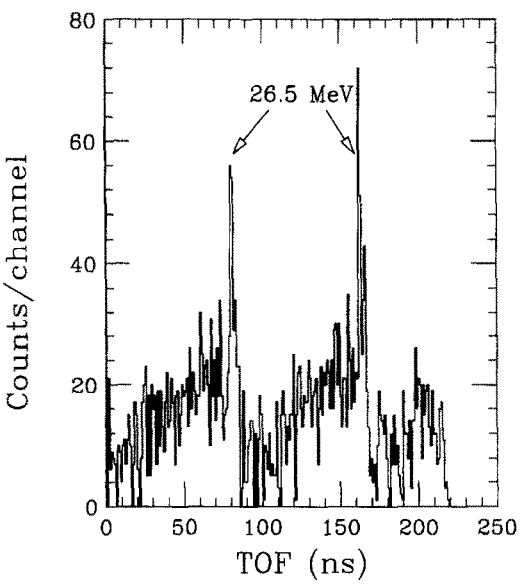

Fig. 9. Time-of-flight spectrum for neutrons detected in cell #7 in the ^{7}Li(p, n) experiment.l The signal of cell #7 gave the start and the downscaled cyclotron radio frequency signal gave the stop. The sharp peaks are from neutrons produced in the reactions leading to either the ground state or the first excited state of ^{7}Be.

TOF. Simulations were carried out only for the neutrons under the sharp peaks because their differential cross-sections were well measured and those neutrons follow simple 2-body kinematics.

Here is how we treat each cross-talk event.

(a) Check for neutron pulses by n-γ discrimination [5]. Reject any γ-ray or cosmic ray events.

(b) Determine the neutron scattering angle θ by the positions of the two scatterings. From the two positions, $(\cos\theta)_m$ is determined.

(c) Determine the ^{7}Li(p, n) reaction angle by the position of the first scattering. From the reaction angle, the incident neutron energy E_n is calculated.

(d) Determine E_p, the energy of the recoil proton in the first scattering, using the geometric mean of the pulse heights from the phototubes at the ends of the cell. PH_l and PH_r denote the pulse heights read out at the left and right ends of the cell, and PH_g denotes the geometric mean. Due to the light attenuation in the NE-213 scintillator, PH_l and PH_r are dependent upon the location of the interaction in the cell: $PH_l \propto I_0 \exp(-x/\lambda)$ and $PH_r \propto I_0 \exp(-(L+x)/\lambda)$, where I_0 is the light intensity, x is the distance light travels from where it is produced to the left end of the cell, L is the length of the cell, λ is the light attenuation length in such the scintillator. PH_g is given by

$$PH_g = (PH_l \times PH_r)^{1/2} \propto I_0 \exp(-L/2\lambda). \quad (10)$$

Since L and λ are constants, PH_g is proportional to the light produced in the scintillator, and is independent of the location of the interaction in the cell. In order to determine the light production of protons in terms of MeVee, each cell was calibrated with the 2.38 MeV Compton edge of a ^{228}Th source and the 4.2 MeV Compton edge of a Pu–Be source. After the light output of each proton is determined, we use Eq. (3) to extract the proton energy E_p.

(e) Calculate $(\cos\theta)_c$ from Eq. (4) with E_n and E_p obtained from (c) and (d).

(f) Determine ΔT_c from Eq. (6) with E_n, E_p and the position of the two scatterings.

(g) ΔT_m, the time difference between the scatterings, was measured in our experiment. In some experiments, $(TOF)_1$ and $(TOF)_2$, the TOFs of the first scattering and the second scattering, respectively, are measured. Then ΔT_m is obtained by subtracting $(TOF)_1$ from $(TOF)_2$ (Eq. 7).

Following the procedure from (a) to (g), we get $(\cos\theta)_c - (\cos\theta)_m$ and $\Delta T_c - \Delta T_m$ for each 2-n event.

5.3. Results

In Fig. 10, the $(\cos\theta)_c - (\cos\theta)_m$ and $\Delta T_c - \Delta T_m$ distributions for those neutrons under the sharp peaks in Fig. 9 are plotted with the open symbols. The histograms are the results of our simulation. All the histograms are normalized according to the areas covered by the data points. Our simulation results are in good agreement with the experimental data. The data points in plot (a) are not exactly centered at zero, as the histogram is. The shift of 0.025 may be due to some error in the measurement of the proton energy. Using Eqs. (1) and (2), we found that a systematic overestimation of 0.65 MeV in E_p could cause the 0.025 shift in the $(\cos\theta)_c - (\cos\theta)_m$ distribution. Two possible sources of this overestimate are an error of a few percent in the light response function [8] or in the proton beam energy. Otherwise, all the measured features of the cross-talk agree with the features in the simulation.

Fig. 11 shows the distribution for all the neutron cross-talk events, those initiated by the 2-body reaction (Eq. (8) and the sharp peaks in Fig. 9) and those initiated by 3-body reaction (Eq. (9) and the continuum neutrons in Fig. (9)), are similar but somewhat broader than those for the 2-body reaction alone.

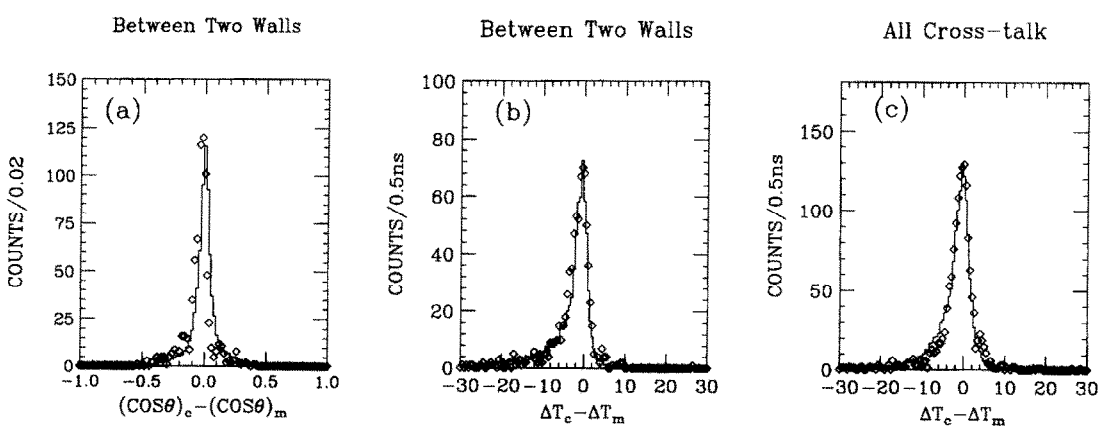

Fig. 10. Cross-talk distributions for the neutrons under the sharp peaks in Fig. 9 from the ^{7}Li(p, n) experiment. The experimental data are given by open symbols. The histograms are the results of our simulation. (a) $(\cos\theta)_c - (\cos\theta)_m$ distribution for the cross-talk events between the two walls. (b) $\Delta T_c - \Delta T_m$ distribution for the same events in (a). (c) $\Delta T_c - \Delta T_m$ distribution for all the cross-talk events.

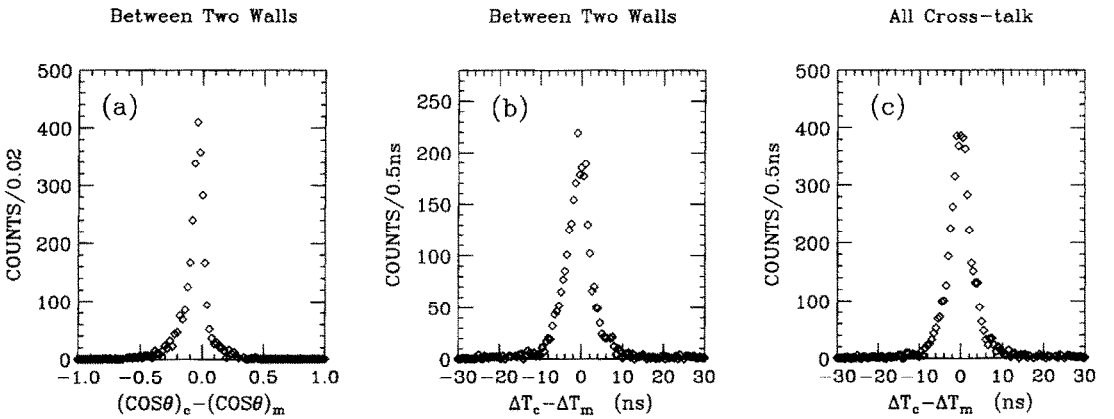

Fig. 11. Cross-talk distributions for all the neutrons from the ^{7}Li(p, n) experiment – those from the 2-body reaction (Eq. (8)) and those from the 3-body reaction (Eq. (9)). (a) $(\cos\theta)_c - (\cos\theta)_m$ distribution for the cross-talk events between the two walls. (b) $\Delta T_c - \Delta T_m$ distribution for the same events in (a). (c) $\Delta T_c - \Delta T_m$ distribution for all the cross-talk events.

6. Summary

A method has been introduced to identify the cross-talk events in multi-detector systems in the energy region up to 25 MeV. In this method, three signatures of cross-talk, $(\cos\theta)_c - (\cos\theta)_m = 0$, $\Delta T_c - \Delta T_m = 0$ and $E'_p \leqslant E'_n$, were established using the n–p elastic scattering kinematics. The three signatures were then studied by a Monte-Carlo simulation. Following the identification procedure presented in the paper, we reject 79% of the neutron cross-talk events in a simulated ^{11}Li breakup experiment. The cross-talk effect was significantly reduced.

A ^{7}Li(p, n) experiment was performed to check our simulation code. The $(\cos\theta)_c - (\cos\theta)_m$ and $\Delta T_c - \Delta T_m$ distributions from Monte-Carlo simulation were compared with experimental data. The consistency between the experimental data and the simulation results prove that neutron cross-talk identification can be achieved in 2-n coincidence experiments.

Our method is based on the 2-body kinematics. In principle, it can be applied to identify neutron cross-talk in any organic multi-detector system. How well it works depends on the specific configuration and the neutron energy.

Acknowledgements

The support of the US National Science Foundation under Grant INT-13997 and PHY92-14992, of The Ministry of Education, Science, Sports and Culture, Japan under Grant 07640421,08640392 and 08044095, and of the Hungarian Academy of Sciences under Grant OTKA 2181 is gratefully acknowledged.

References

[1] L. Lüdemann, K. Knoche, W. Scobel, K. Woller, Nucl. Instr. and Meth. A 334 (1993) 495.
[2] P. Désesquelles, A.J. Cole, A. Dauchy, A. Giorni, D. Heuer, A. Lleres, C. Morand, J. Saint-Martin, P. Stassi, J.B. Viano, B. Chambon, B. Cheynis, D. Drain, Nucl. Instr. and Meth. A 307 (1991) 366.
[3] A.V. Kuznetsov, I.D. Alkhazov, D.N. Vakhtin, V.G. Lyapin, V.A. Rubchenya, W.H. Trzaska, K. Loberg, A.V. Daniel, Nucl. Instr. and Meth. A 346 (1994) 259.
[4] M. Cronqvist, B. Jonson, T. Nilsson, G. Nyman, K. Riisager, H.A. Roth, Ö. Skeppstedt, O. Tengblad, K. Wilhelmsen, Nucl. Instr. and Meth. A 317 (1992) 273.
[5] R. Ghetti, L. Carlén, M. Cronqvist, B. Jakobsson, F. Merchez, B. Norén, D. Rebreyend, M. Rydehell, Ö. Skeppstedt, L. Westerberg, Nucl. Instr. and Meth. A 317 (1992) 273.
[6] D. Sackett, K. Ieki, A. Galonsky, C.A. Bertulani, H. Esbensen, J.J. Kruse, W.G. Lynch, D.J. Morressy, N.A. Orr, B.M. Sherrill, H. Schulz, A. Sustich, J.A. Winger, F. Deák, A. Horváth, Á. Kiss, Z. Seres, J.J. Kolata, R.E. Warner, D.L. Humphrey, Phys. Rev. C 48 (1993) 118.
[7] P.D. Zecher, A. Galonsky, J.J. Kruse, J. Wang, F. Deák, S.J. Gaff, Á. Horváth, K. Ieki, Y. Iwata, Á. Kiss, J. Ottarson, H. Schelin, Z. Seres, Nucl. Instr. and Meth., submitted.
[8] V.V. Verbinski, W.R. Burrus, T.A. Love, W. Zobel, N.W. Hill, R. Textor, Nucl. Instr. and Meth. 65 (1968) 8.
[9] R.A. Cecil, B.D. Anderson, R. Madey, Nucl. Instr. and Meth. 161 (1979) 439.